International Journal of Bifurcation and Chaos, Vol. 22, No. 3 (2012) 1230012 (12 pages)

DOI: 10.1142/S0218127412300121

MEASURABLE DYNAMICS ANALYSIS OF TRANSPORT IN THE GULF OF MEXICO DURING THE OIL SPILL

ERIK M. BOLLT*, AARON LUTTMAN†, SEAN KRAMER‡
and RANIL BASNAYAKE§
Department of Mathematics, Clarkson University,
Box 5815, Potsdam, NY 13699, USA
**bolltem@clarkson.edu*
†*aluttman@clarkson.edu*
‡*kramersj@clarkson.edu*
§*basnayrk@clarkson.edu*

Received December 23, 2010

On April 20, 2010, an oil well cap explosion below the *Deepwater Horizon*, an off-shore oil rig in the Gulf of Mexico, started the worst human-caused submarine oil spill ever. Though an historic tragedy for the marine ecosystem, the unprecedented monitoring of the spill in real time by satellites and increased modeling of the natural oceanic flows has provided a wealth of data, allowing analysis of the flow dynamics governing the spread of the oil. In this work, we present the results of two computational analyses describing the mixing, mass transport, and flow dynamics of the oil dispersion in the Gulf of Mexico over the first 100 days of the spill. Transfer operator methods are used to determine the spatial partitioning of regions of homogeneous dynamics into almost-invariant sets, and Finite Time Lyapunov Exponents are used to compute pseudo-barriers to the mixing of the oil between these regions. The two methods give complementary results, generating a comprehensive description of the oil flow dynamics over time.

Keywords: Finite time Lyapunov exponent; Fröbenius–Perron operator; fluid mixing; Gulf oil spill; applied dynamical system; chaotic dynamics.

1. Introduction

Two pressing, yet related, problems in the general study of fluid dynamics are understanding mixing mechanisms and modeling transport. Both are of special concern in oceanic systems, where large-scale and local flow dynamics partition the seascape into distinct regions, and agents and pollutants can advect from one such region to another, critically impacting ecologies, peoples, and economies. Understanding and describing these distinct regions and the transport of pollutants between them can be considered a "pre-processing" step to controlling the spread of unwanted chemicals. The importance of such fundamental questions of fluid dynamics was unfortunately publicly and widely underscored by the oil spill disaster in the Gulf of Mexico during the spring and summer of 2010 [Aigner *et al.*, 2010]. Following the initial explosion beneath the *Deepwater Horizon* drilling rig on April 20, 2010, oil continued to spill into the Gulf of Mexico from the resulting fissure in the well head on the sea floor. Spill rates have been estimated at 53 000 barrels per day by the time the leak was controlled by the "cap" three months later. It is estimated that

*Author for correspondence

approximately 4.9 million barrels, or 185 million gallons of crude oil flowed into the Gulf of Mexico, making it the largest-ever submarine oil spill. The regional damage to marine ecology was extensive, but the impacts were seen on much larger scales as well, as some oil seeped into the Gulf Stream, which transported the oil around Florida and into the Atlantic Ocean. Initially, the amount of oil that would disperse into the Atlantic was overestimated, because a prominent dynamical structure arose in the gulf early in the summer preventing oil from entering the Gulf Stream. Computational tools for analyzing the transport mechanisms governing the advective spread of the oil are the subject of this paper. Figure 1 shows a satellite image of the Gulf of Mexico off the coast of Louisiana on May 24, 2010. The oil is clearly visible in white in the center of the image, and the spread of the oil can already be seen, just over a month after the initial explosion. During the early days of the spill, the Gulf Stream was draining oil out of the gulf and, eventually, into the Atlantic. This spread was substantially tempered later in the summer, due to the development of a natural eddy in the central Gulf of Mexico, which acted as a barrier to transport.

It is in the setting of this tragedy that we study the flow dynamics in the gulf, using vector fields generated from a model describing the oceanic flows during the time of the spill. The data set used in these simulations is from the Hybrid Coordinate Ocean Model (HYCOM), a PDE model describing oceanic flow. The data generated by this model has been produced out of a multi-institutional effort sponsored by the National Ocean

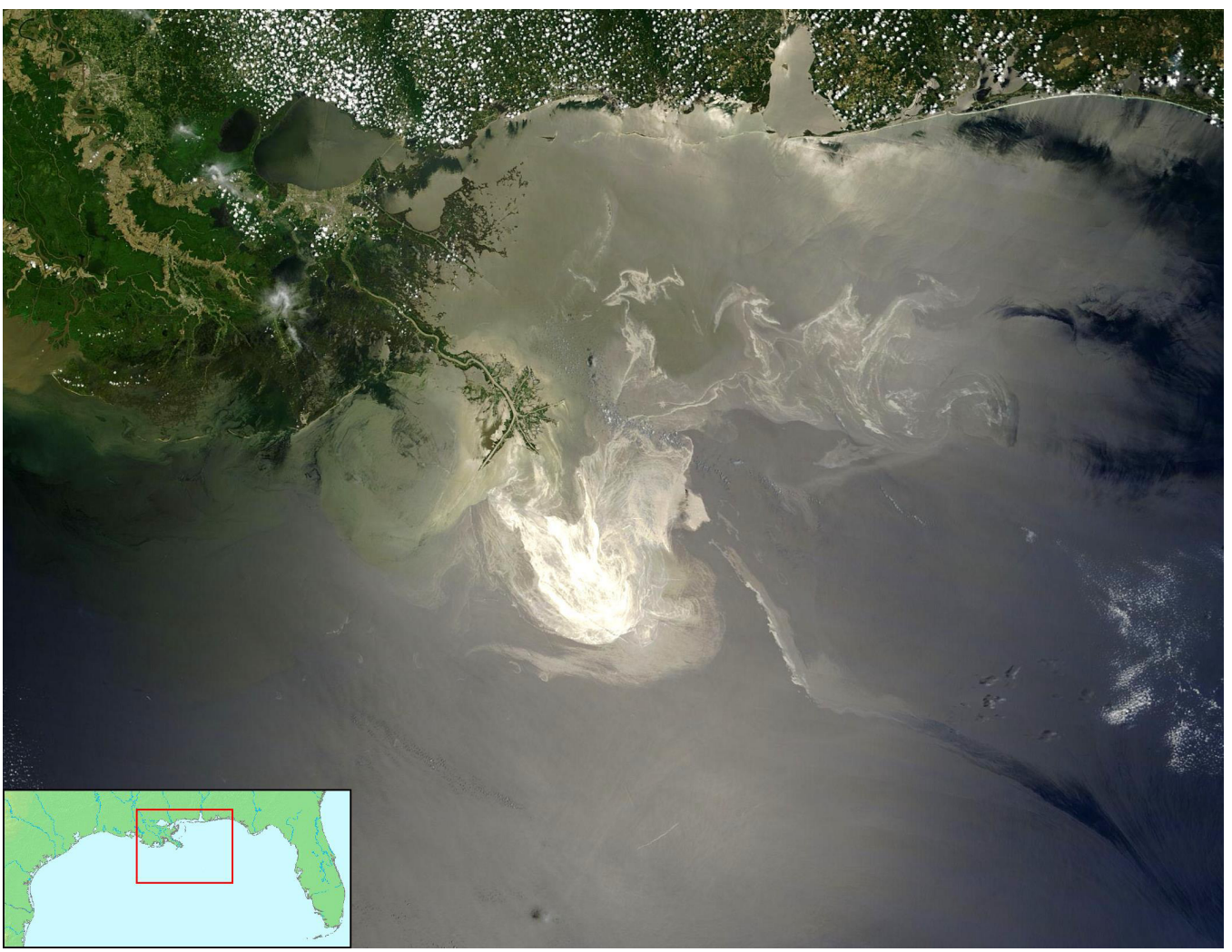

Fig. 1. Satellite view of the Gulf of Mexico near Louisiana during the oil spill disaster, May 24, 2010. The oil slick spread is clearly visible and large. The image, taken by NASA's Terra satellite, is in the public domain.

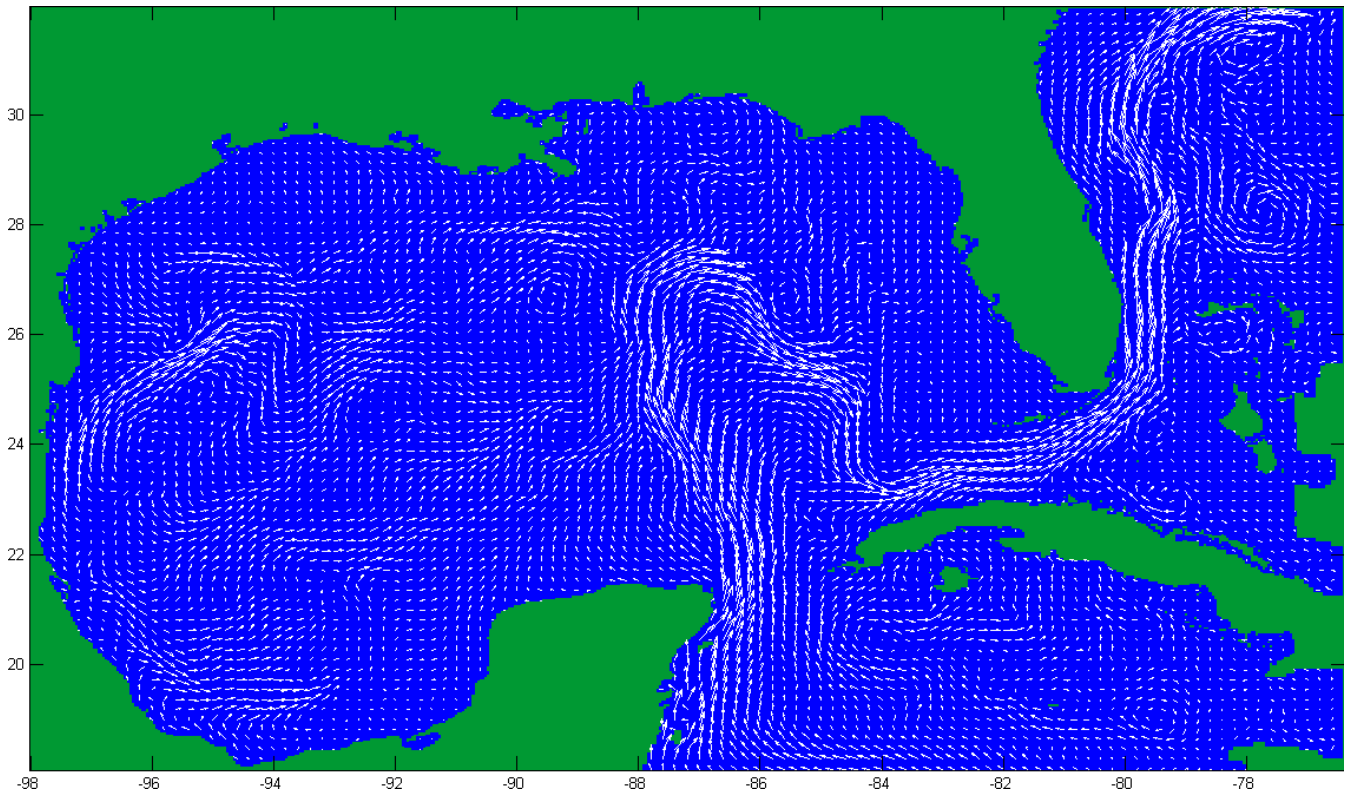

Fig. 2. Vector field describing surface flow in the Gulf of Mexico on May 24, 2010, computed using the HYCOM model [HYCOM, 2010]. Note the coherence of the Gulf Stream at this time. Oil spilling from south of Louisiana could flow directly into the Gulf Stream and out towards the Atlantic. Horizontal and vertical units are degrees longitude (negative indicates west longitude) and degrees latitude (positive indicates north latitude), respectively.

Partnership Program (NOPP) and is publicly available [HYCOM, 2010]. The scientific details of the model are described, e.g. in [Bleck, 2002; Halliwell, 2004]. The objectives of the consortium include real-time, three-dimensional depictions of ocean products such as sea surface temperature, salinity, and currents for the Atlantic and Pacific oceans. The form of the data is a nonautonomous, three-dimensional vector field

$$\mathbf{f} : \mathbb{R}^3 \times \mathbb{R}^+ \to \mathbb{R}^3$$

$$\mathbf{f}(x, y, z, t) = \langle u(x, y, z, t), v(x, y, z, t), w(x, y, z, t) \rangle,$$

at longitude and latitude positions x and y, depth z, and time t. Figure 2 shows the HYCOM modeled flow on the surface of the Gulf of Mexico on May 24, 2010. The fundamental dynamical structure in this image is the Gulf Stream, which can be backtracked from the northeast corner of the image, around the horn of Florida, back up into the central Gulf of Mexico, then down around the Yucatan Peninsula. During the initial days of the oil spill, this was the driving system governing the spread of oil, but that changed later in the summer when another dynamical structure arose. The impact of these structures on the oil transport will be demonstrated and quantified in the sections that follow.

In order to develop a comprehensive description of the mixing and transport in the Gulf of Mexico over this time period using the data provided by the HYCOM model, we will pursue the following two complementary methods of analysis of transport mechanisms:

- Finite Time Lyapunov Exponents (FTLE), and
- Transfer operator methods based on discretizing the Fröbenius–Perron operator.

Each of these approaches is described briefly in subsequent sections, and results specialized to the setting of the Gulf of Mexico during the crisis are presented in the section that follows.

2. Transport Barriers and the FTLE Analysis

In this section we review the analysis of transport and mixing via Lagrangian coherent structures

(LCS) based on Finite Time Lyapunov Exponents (FTLE) [Haller & Poje, 1998; Haller, 2000, 2002]. For a steady flow, the LCSs extracted from the FTLE field approximate stable and unstable invariant manifolds of a hyperbolic fixed point. Both invariant manifolds of a separatrix heteroclinic connection are generally understood to moderate transport in dynamical systems, in what has become a classical theory of global dynamics [Meiss, 1992; Wiggins, 1992]; these manifolds separate regions exhibiting qualitatively different activities. A driving viewpoint is that FTLEs approximately represent these structures, as the ridges describe sets across which there is slow diffusion [Shadden *et al.*, 2005], although with some important recent caveats [Shadden *et al.*, 2009]. Moreover, as opposed to the stable and unstable manifolds — and fundamental to applications — FTLEs are readily computed when the dynamical system is known only through empirical measurements.

In general, if LCSs are of co-dimension one relative to the domain of the dynamical system, they constitute pseudo-barriers to transport and mixing, which is to say the flux of particles across an LCS approaches zero as the integration time for computation of the FTLE becomes large [Shadden *et al.*, 2005, 2006]. A practical approach to locating LCSs is to compute the FTLE of a time-dependent velocity field, quantifying the local stretching rate over a finite time interval [Haller, 2000, 2002].

Given a velocity field $\mathbf{v}(\mathbf{x}, t)$ on a manifold $M \subset \mathbb{R}^d$,

$$\frac{d\mathbf{x}}{dt} = \mathbf{v}(\mathbf{x}, t) \tag{1}$$

where $\mathbf{x} \in M$ and $\mathbf{v}(\mathbf{x}, t)$ is at least $C^2(M)$ — integrating yields the flow map $\phi_t \colon \mathbf{x}(t) \mapsto \mathbf{x}(t + \tau)$. The finite-time strain tensor of the velocity field along the trajectory $\mathbf{x}(t)$ is given by the symmetric, time-dependent, $d \times d$ matrix

$$J_\tau = \left[\frac{d\phi_\tau \mathbf{x}(t)}{d\mathbf{x}}\right]^* \frac{d\phi_\tau \mathbf{x}(t)}{d\mathbf{x}}, \tag{2}$$

where A^* denotes the adjoint of A. In the sequel we assume that $d = 2$, but this assumption is only for ease of presentation and not mathematically necessary.

If over a finite time interval $[t, t + \tau]$, the minimum and maximum eigenvalues, $\lambda_{\min}(\tau)$ and $\lambda_{\max}(\tau)$, of J_τ satisfy the condition

$$\ln \lambda_{\min}(\tau) < 0 < \ln \lambda_{\max}(\tau), \tag{3}$$

then the canonical local material advective behavior is described by circles evolving into ellipses, where the major axis determines the orientation of instability. This condition implies that there is compression in one direction and expansion in the other along the trajectory. This type of trajectory in a time-dependent velocity field is referred to as a *hyperbolic trajectory*.

Recall that the spectral norm of the Jacobian, $\frac{d\phi_\tau \mathbf{x}(t)}{d\mathbf{x}}$, is given by

$$\left\| \frac{d\phi_\tau \mathbf{x}(t)}{d\mathbf{x}} \right\|^2 = \lambda_{\max}(\tau). \tag{4}$$

Then the FTLE, which represents the maximum stretching at the point $\mathbf{x}(t)$ along the trajectory with duration time τ, is given by

$$\begin{aligned} \sigma_\tau(\mathbf{x}(t)) &= \frac{1}{|\tau|} \ln \left\| \frac{d\phi_\tau \mathbf{x}(t)}{d\mathbf{x}} \right\| \\ &= \frac{1}{|\tau|} \ln \sqrt{\lambda_{\max}(\tau)}. \end{aligned} \tag{5}$$

The repelling and attracting LCSs are then defined as the maximum ridges of the FTLE computed in forward time ($\tau > 0$) and backward time ($\tau < 0$), respectively [Haller, 2002; Shadden *et al.*, 2005].

2.1. *FTLE in the Gulf*

The HYCOM data set is a finite array of values, $\mathbf{v}(\mathbf{x}, t)$, sampled on a grid of geographic positions in the ocean, $\mathbf{x}$, at discrete times t. Integration of the vector field in (1) and the associated tangent bundle in (2) each require samples of the vector field at positions in between the grid values. Super resolution is needed, and the interpolation is performed using (generally) stiff cubic smoothing splines, where a great deal of stiffness weighs the balance toward strong agreement with the data.

Figure 3 shows the computed FTLE for the vector field $\mathbf{v}(\mathbf{x}, t)$, beginning on April 20, 2010, using a 3-day window (i.e. $\tau = 3$ days). In this representation, red indicates ridges of the scalar field, transverse to which little diffusion will occur, by the theory in [Shadden *et al.*, 2005]. The striking large-scale regions are the loop-and-circulation just northwest of Cuba and the expected boundaries of the Gulf Stream north of Cuba and northward east of Florida. The implication of this computation is that outlining these regions is a likely partition of dynamical relevance.

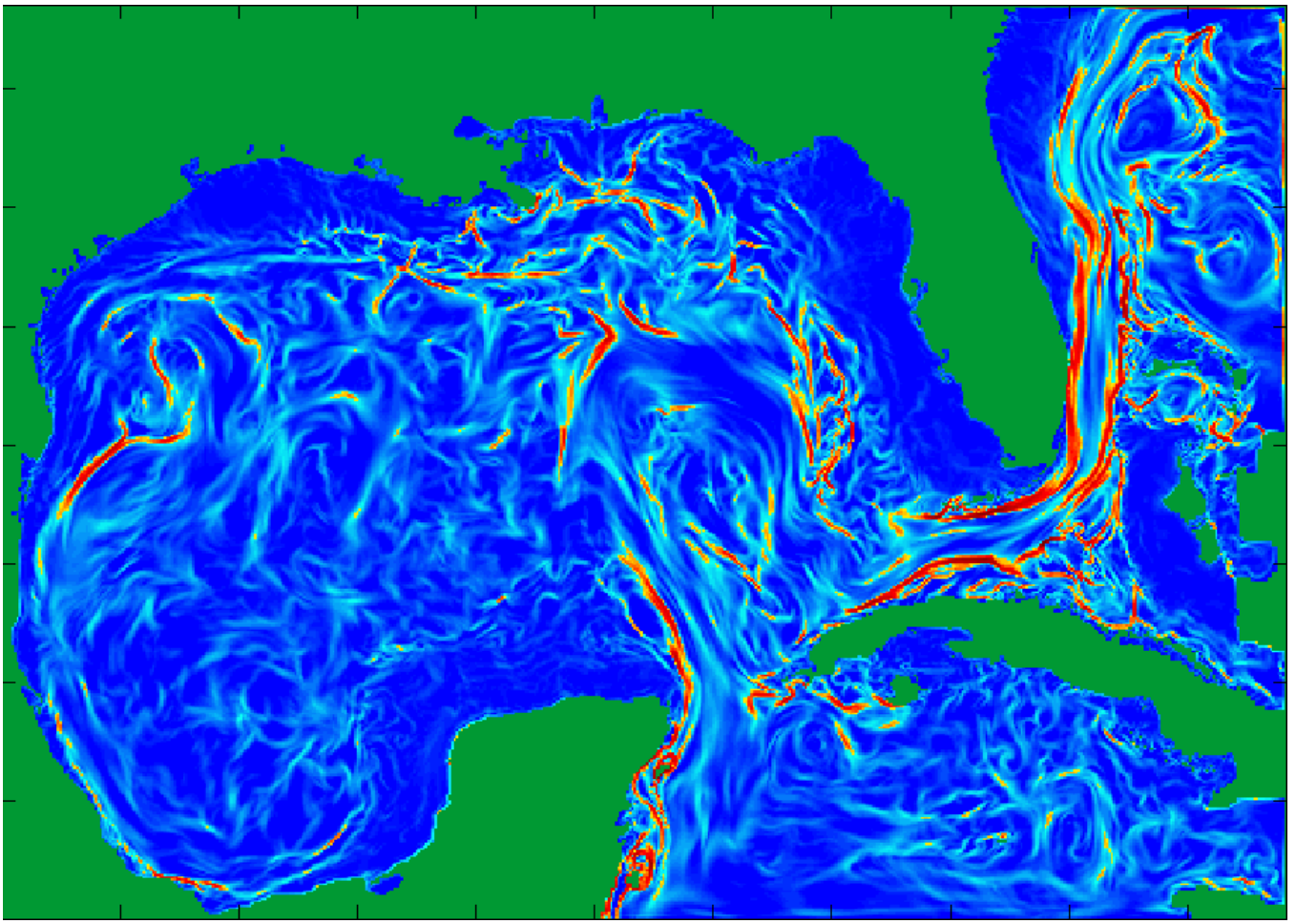

Fig. 3. FTLE for the Gulf computed from a 3-day range starting on April 20, 2010, derived from HYCOM data. The red regions denote the strongest barriers to transport and generally outline components partitioning almost invariance.

What cannot be readily seen from a static snapshot of the FTLE field is its time varying nature, due to the fact that the driving vector field is nonautonomuous. A movie of the time evolution of the FTLE field from April 20, 2010, to July 28, 2010, is available online[1] [Bollt *et al.*, 2010], and it shows that the red ridges corresponding to approximate transport barriers form pockets and walls that push the oil (represented as ensembles of initial conditions being flowed from the oil spill source) around the Gulf. Given that Fig. 3 represents the first three days of the oil spill, only a small amount of oil has flowed out of the immediate vicinity of the spill source, so the ensembles of initial conditions are not displayed. Roughly halfway through the 100-day period used in the computations, the FTLEs open and pull the ensembles through to more southerly parts of the Gulf, whereafter it would appear the advective tendency is to shuttle fluid into the Gulf stream and eventually northward. This behavior is shown in Fig. 4, which displays the FTLE field for the 3-day window, beginning May 24, 2010, the same day as is shown in the satellite image in Fig. 1. Note the evolution of the transport barriers. As it turned out, the evolution of the transport barriers was more complex than was initially estimated, and large-scale transport of oil into the Gulf Stream did not occur.

Overlayed on the FTLE in Fig. 4 is the underlying vector field $\mathbf{v}(\mathbf{x}, t)$ for May 24, 2010, which is the beginning of the 3-day frame of integration used to compute the FTLE, and we emphasize that the vector field is not universally parallel to the ridges. Also shown is a sample of black tracers representing oil as if it had been advected from the origin of the spill through the 34-day time period up until the

[1]http://people.clarkson.edu/∼aluttman/GulfFTLE.mov

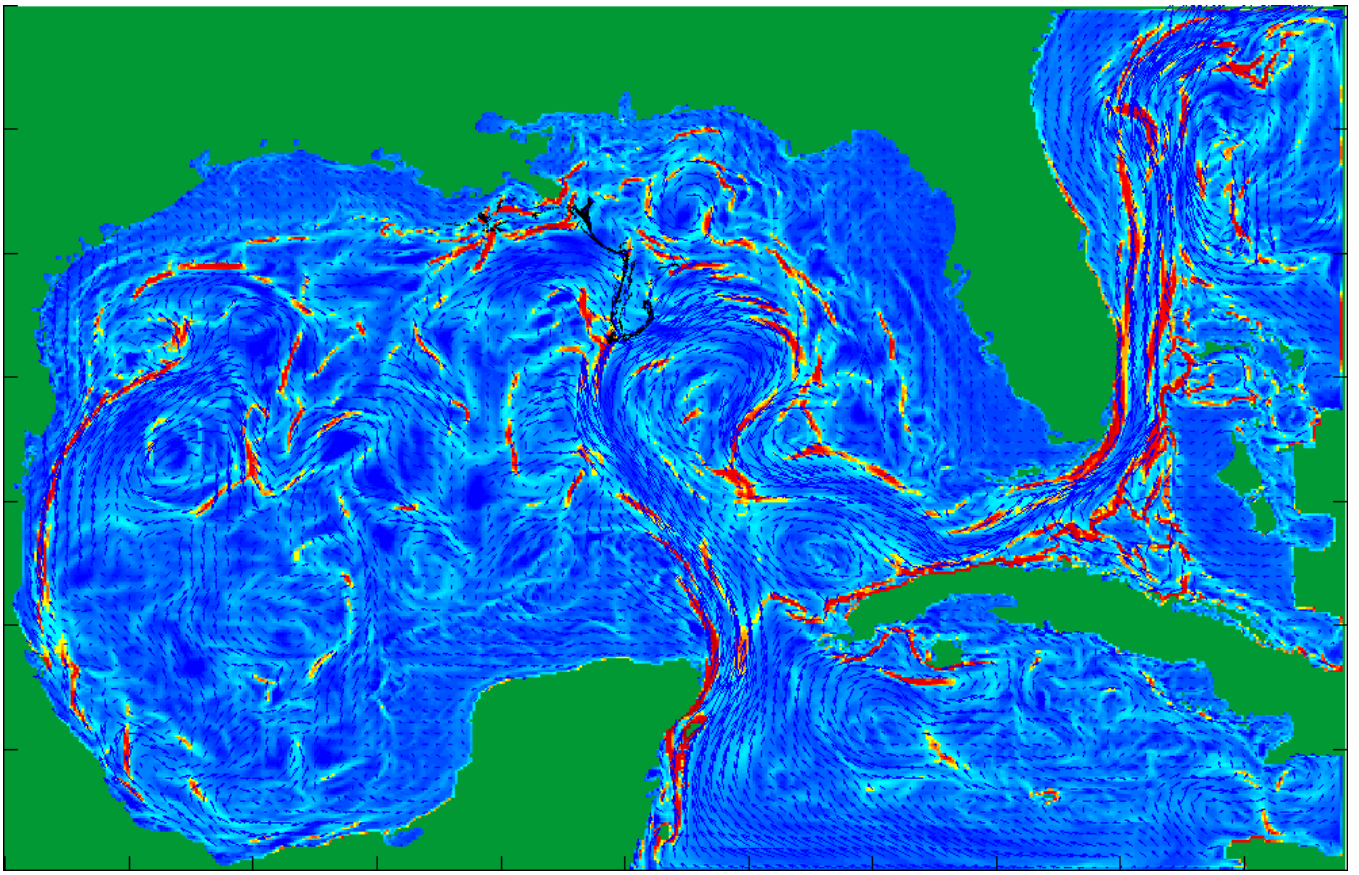

Fig. 4. FTLE for the Gulf computed from a 3-day range beginning May 24, 2010. Contrast to Fig. 3, which shows the transport pseudo-barriers at an earlier date. Also shown is the underlying vector field on May 24, 2010, as well as black tracers representing the spread of oil. A month after the initial explosion, the tracer particles have dispersed significantly from the source.

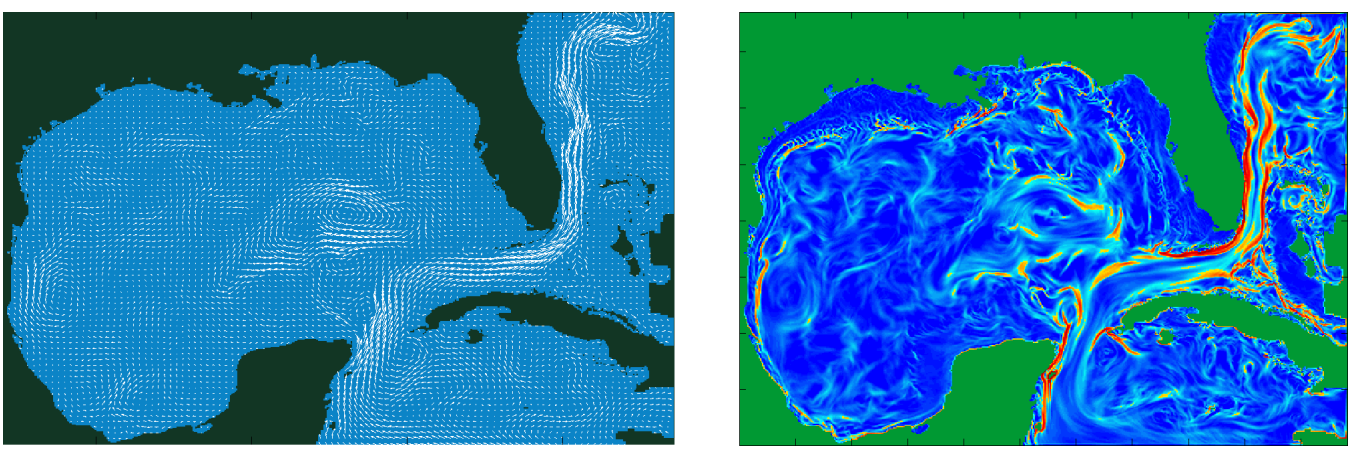

Fig. 5. The HYCOM vector field and associated FTLE for July 27, 2010. The central eddy in the Gulf of Mexico can be clearly seen in the vector field, and the associated transport boundaries are evident in the FTLE. Note the difference in the flow field from that shown in Fig. 2, where the Gulf Stream was directly connected to the central flow. Now the central eddy has broken from the Gulf Stream, cutting off the oil transport into the Gulf Stream. This is clear in the FTLE field, as due west of Florida are two orange ridges representing the barrier to oil transport. This barrier prevented large amounts of oil from entering the Gulf Stream and transporting into the Atlantic Ocean during the summer months of 2010.

day shown. The main feature to emphasize is how the tracers manage to weed their way through the FTLE mostly along the red ridges and not transversely, thus obeying the principle of low transverse diffusion. It is through the openings in these ridges that the oil must shuttle, if it is to transport. Figure 4 also shows a ridge blocking entrance into the Gulf Stream that has arisen due to the strong circulation in the middle of the Gulf. This ridge represents the "Eddy Franklin," a recurring eddy that forms in the central Gulf of Mexico. This structure can be seen more clearly in Fig. 5. On the left we have the HYCOM vector field computed for July 27, 2010. The vector field clearly shows the eddy to the northwest of Cuba. On the right in Fig. 5 is the corresponding FTLE field, which demonstrates the barrier between the region south of Louisiana, from which the oil was flowing, and the Gulf Stream. This dynamical structure prevented oil from entering the Gulf Stream on a large scale and greatly reduced the amount of oil that dispersed into the Atlantic Ocean.

3. Transfer Operator Methods for Inferring Components

While the FTLE suggests pseudo-barriers to transport, the interior regions bounded by the FLTE ridges are the topological partition elements, and transfer operator methods are ideally suited for inferring these interiors directly. Moreover, computed via transfer operators, these partition elements have a more direct principled mathematical relationship to almost invariant sets.

3.1. *Fröbenius–Perron and Koopman operators*

Let $(\mathbb{X}, \mathbb{A}, \mu)$ be a measure space and $F\colon \mathbb{X} \to \mathbb{X}$ a non-singular, measurable transformation on $(\mathbb{X}, \mathbb{A}, \mu)$ such that $\mu(F^{-1}(A)) = 0$ for each $A \in \mathbb{A}$ satisfying $\mu(A) = 0$. The *Fröbenius–Perron operator*, $P\colon L^1(\mathbb{X}) \to L^1(\mathbb{X})$ with respect to F is defined by

$$Pf(x) = \int_{\mathbb{X}} \delta(x - F(y)) f(y) dy, \tag{6}$$

where $f(x) \in L^1(\mathbb{X})$ is a probability density function (PDF) [Lasota & Mackey, 1994] and $\delta(x)$ is the point of mass distribution. Thus $Pf(x)$ gives a new PDF, which depends on the discrete-time transformation F and the probability density function $f(x)$ and is unique almost everywhere (a.e.). The Fröbenius–Perron operator satisfies the discrete-time continuity equation

$$\int_{F^{-1}(A)} f(x)dx = \int_A Pf(x)dx \tag{7}$$

for each measurable set $A \in \mathbb{A}$ [Lasota & Mackey, 1994].

The *Koopman Operator*, $K\colon L^\infty(\mathbb{X}) \to L^\infty(\mathbb{X})$, with respect to F is defined by

$$Kg(x) = g(F(x)) \tag{8}$$

for $g \in L^\infty(\mathbb{X})$. In this context, the key property of the Koopman operator is that it is the adjoint of the Fröbenius–Perron operator. That is for every $\rho \in L^1(\mathbb{X})$ and $g \in L^\infty(\mathbb{X})$

$$\langle P\rho, g\rangle = \langle \rho, Kg\rangle, \tag{9}$$

where we denote the bilinear form $\langle\cdot,\cdot\rangle_{L^1(\mathbb{X})\times L^\infty(\mathbb{X})}$ by $\langle\cdot,\cdot\rangle$ here throughout.

Defining a discrete-time mapping F from the flow given by (1) — specifically for the simulations presented here based on the HYCOM data of the Gulf of Mexico — may be understood as a standard stroboscopic Poincaré mapping. In this case, $\mathbb{X}$ is the Gulf of Mexico, and the mapping $F \equiv \phi_t(\mathbf{x})$ is defined in terms of the flow operator ϕ_t. In practice, a numerical integration scheme is used, and splines are used to interpolate the vector field between data points for the ODE solver, as discussed above. It is straightforward to construct subroutines that effectively implement the stroboscopic mapping F for a given, fixed time window $t_0 \le t \le t_f$. From this implementation of F, the next section concerns numerically estimating the infinite-dimensional Fröbenius–Perron operator.

3.2. *Finite-rank approximation*

We compute a discrete approximation to the Fröbenius–Perron operator using the Ulam–Galerkin method [Ulam, 1970; Li, 1976]. Assume that $\mathbb{X}$ has finite Lebesgue measure — so that $L^2(\mathbb{X}) \subset L^1(\mathbb{X})$ — and let $\{\phi_i\}_{i=1}^\infty \subset L^2(\mathbb{X})$ be a complete orthonormal system (see e.g. [Wheeden & Zygmund, 1977] for terminology). Then we approximate a function $f \in L^2(\mathbb{X})$ by its orthogonal projection onto the finite-dimensional subspace

$$\triangle_N = \text{span}\{\phi_i(x)\}_{i=1}^N. \tag{10}$$

For Galerkin's method, this projection,

$$\Pi\colon L^1(\mathbb{X}) \to \triangle_N, \tag{11}$$

maps a function from an infinite-dimensional space down into a finite-dimensional function space. Thus, given the operator $P\colon L^1(\mathbb{X}) \to L^1(\mathbb{X})$ restricted to $L^2(\mathbb{X})$, the composition of P with the projection, $P \circ \Pi$, results in an operator of finite rank, represented by an $N \times N$ matrix, via the inner product

$$A_{i,j} = \langle P\phi_i, \phi_j \rangle = \int_{\mathbb{X}} P\phi_i(x)\phi_j(x)dx. \tag{12}$$

The quality of the approximation of P by $P \circ \Pi$ is discussed in many references including [Chui *et al.*, 1992; Ding & Zhou, 1994; Hunt, 1996].

The region $\mathbb{X}$ is represented by a covering of closed sets $\{B_i\}_{i=1}^N$. In principle, this representation can consist of any collection of closed sets satisfying $\text{int}(B_i) \cap \text{int}(B_j) \neq \varnothing$ for $j \neq i$ and $\mathbb{X} \subset \cup_i B_i$, though in practice it is constructed in a straightforward way. In order to ensure a prescribed degree of accuracy for the Ulam–Galerkin representation, we first define a threshold $\epsilon_{\max}$, then the closed sets B_i should be chosen with $\text{diam}(B_i) < \epsilon_{\max}$. It is also helpful to choose conveniently shaped regions, such as rectangles or triangles. In practice, we use a Delaunay triangulation of the underlying domain, as such a decomposition is straightforward to work with from a programming standpoint in that it lends itself nicely to an iterative, adaptive refinement.

Ulam's method [Ulam, 1970] is a special case of Galerkin's method, where the basis functions are a family of characteristic functions,

$$\begin{aligned}\phi_i(x) &= \chi_{B_i}(x) \\ &= 1 \quad \text{for } x \in B_i \text{ and zero otherwise.}\end{aligned} \tag{13}$$

It is interesting to note that in certain applications it may be useful to use different complete orthonormal systems for $L^2(\mathbb{X})$, for example, using basis functions such as wavelets. The traditional Ulam method concerns weak convergence for a computed invariant measure, which is a process incorporating behavior over the long-term. This contrasts with the computational use of Galerkin's method, which is used widely and here, which concerns only the short-term, one-step accuracy of the representation. This is a much simpler problem to analyze. Using (12), the matrix approximation of the Fröbenius–Perron operator has the form of

$$A_{i,j} = \frac{m(B_i \cap F^{-1}(B_j))}{m(B_i)}, \tag{14}$$

where m denotes the Lebesgue measure on $\mathbb{X}$ (as opposed to μ, which denotes the natural, invariant measure on $\mathbb{X}$). Now m can be estimated simply, for example using Monte-Carlo simulations, whereas the estimation of μ takes greater care.

The entries $A_{i,j}$ can be interpreted as the ratio of the fraction of the box B_i that will be mapped to the box B_j to a measurement of the "size" of B_i. Note that if we only have a test orbit $\{x_j\}_{j=1}^N$ — which is actually the main interest of this paper — the Lebesgue measure can be approximated by a counting measure λ and the matrix approximation of the Fröbenius–Perron operator becomes

$$A_{i,j} = \frac{\lambda(\{x_k | x_k \in B_i \text{ and } F(x_k) \in B_j\})}{\lambda(\{x_k \in B_i\})}. \tag{15}$$

4. Partition to Emphasize Almost-Invariance

A fundamental aspect of transport analysis is partitioning the underyling domain into invariant or almost-invariant sets, if they exist. We will consider and review here transport analysis via theories for partitioning graphs, including a discussion of the strengths of each approach for analyzing flux in the dynamical systems these graphs represent. A common scenario in advective turbulent dynamical systems is for the long-time behavior to be transitive (or correspondingly ergodic in terms of measurable dynamics), but the short-time behavior may reveal only slow transport between almost invariant sets [Froyland & Padberg, 2009; Froyland, 2005; Bollt *et al.*, 2002]. Such behavior has been called "weakly transitive" [Froyland, 2005].

The basic idea behind using the finite-rank approximation given in (15) to the transfer operator is that partitions associated with almost invariance correspond to the blocks of the matrix

$$\tilde{A} = P^T A P, \tag{16}$$

where P is a permutation matrix and $\tilde{A}$ is in almost block-diagonal form. That is, finding the partitions corresponds to finding the permuation matrix P such that $\tilde{A}$ is as close to block diagonal as it can get. In particular, $\tilde{A}$ must have the form

$$\tilde{A} = \begin{pmatrix} R_{1,1} & E_{1,2} \\ E_{2,1} & R_{2,2} \end{pmatrix}, \tag{17}$$

where $E_{1,2}$ and $E_{2,1}$ are matrices of "relatively small" Fröbenius norm [Golub & Van Loan, 1996], which is given by

$$\|B\|_F = \sqrt{\mathrm{Tr}(B \cdot B^T)} = \sqrt{\sum_{i=1}^{N}\sum_{j=1}^{N} |b_{i,j}|^2}. \quad (18)$$

More specifically, "relatively small" means that the ratios

$$\frac{\|E_{1,2}\|_F}{\|R_{1,1}\|_F} \quad \text{and} \quad \frac{\|E_{2,1}\|_F}{\|R_{2,2}\|_F}$$

are below some predefined threshold.

There are several popular methods for transforming A into nearly block diagonal form — each of which is formulated as an optimization problem — including community methods [Newman, 2004, 2006], max-flow/min-cut type methods, and reduction of congestion methods [Preis & Dellnitz, 2003]. Another more recent and successful approach is the balanced Markov chain method [Froyland, 2005], derived from the theory of reversible Markov chains and associated with spectral graph theory [Chung, 1997; Chan *et al.*, 1995]. There is a beautiful connection between this method and the spectral version of the graph modularity method stated in its spectral formulation [Newman, 2006]. Here we use a variation of the spectral graph theory method [Chung, 1997]. Assume that A is a stochastic matrix, with dominant eigenvalue $\lambda = 1$ of multiplicity 1 and with eigenvector p. Consider the transition matrix $\overline{A}$ of the time-reversed Markov chain defined by

$$\overline{A}_{i,j} = \frac{p_j A_{j,i}}{p_i}. \quad (19)$$

While this formula is discussed in [Froyland, 2005], we advance the technology by addressing here the likely scenario that $p_i = 0$ for some i by the methods associated to Eqs. (24)–(26) discussed herein. In a matrix form, $\overline{A} = \Pi^{-1} A^T \Pi$, where Π is a diagonal matrix with $\Pi_{i,i} = p_i$. This is defined in [Brémaud, 1999] and discussed in the context of almost invariance with respect to dynamical systems in [Froyland, 2005]. It is easy to check that $p\overline{A} = p$. The *additive reversibilization* of A is defined as

$$R = \frac{1}{2}(A + \overline{A}). \quad (20)$$

The Markov chain represented by the reversibilized transition matrix R is reversible and has p as the stationary distribution as well, i.e. under the dynamics governing the Markov chain R, the probability to go from states i to j is the same as going from states j to i (i.e. $p_i R_{i,j} = p_j R_{j,i}$).

Recall that the normalized graph Laplacian [Chung, 1997] is given by

$$\begin{aligned}\mathcal{L} &:= I - \Pi^{-1/2} R \Pi^{1/2} \\ &= I - \frac{\Pi^{1/2} A \Pi^{-1/2} + \Pi^{-1/2} A^T \Pi^{1/2}}{2}. \end{aligned} \quad (21)$$

It is clear that $\mathcal{L}$ is symmetric, so optimal partitioning comes by applying the Courant–Fischer Theorem to $\mathcal{L}$. More precisely, consider the minimization problem of computing

$$\mathrm{argmin} \frac{x^T (I - \mathcal{L}) x}{x^T x} \quad \text{subject to: } \sum_i x_i p_i^{1/2} = 0. \quad (22)$$

Notice that due to the relation $x = \Pi^{1/2} y$, the optimal vector x has to be constrained to be orthogonal to $p^{1/2}$ for y to be orthogonal to p. Also, we note that, after obtaining the optimal vector x, we have to revert it to y. Following the Courant–Fischer Theorem the optimal partition is derived spectrally by

$$\begin{aligned}\lambda_2 &= \min_{x^T p^{1/2} = 0, x \neq 0} \frac{x^T \mathcal{L} x}{x^T x} \\ &= \min_{y^T p = 0, y \neq 0} \frac{\sum_{i,j} (y_i - y_j)^2 p_i A_{i,j}}{\sum_i y_i^2 p_i}. \end{aligned} \quad (23)$$

This minimum is attained by the eigenvector $x = v_2$, where $y = \Pi^{-1/2} v_2$ corresponds to the second eigenvalue λ_2 of the normalized Laplacian $\mathcal{L}$ (see [Chung, 1997; Brémaud, 1999; Bollt & Santitissadeekorn, 2012]).

A problem with the above is that the spectral graph theory, in terms of the reversible Markov chain and the normalized graph Laplacian, implicitly assumes that the dominant state p used to reverse A has no zero entries, i.e. $p_i > 0$ for each i. This scenario can be easily violated, for example, when the dynamical system is not recurrent. Specifically in our data sets from the Gulf of Mexico, on the largest scale there is a flow due to the Gulf stream. Mass flows into the system in the region south of Cuba and flows out of the system in the

Atlantic, northeast of Florida. This is, of course, due to the fact that the region shown is not a closed subsystem of the world's ocean's as a whole. As a consequence, for each i such that B_i decreases in mass, we have $p_i = 0$. A simple approximate fix to this situation is to replace (19) with,

$$C = \text{ceil}(A), \tag{24}$$

which is an adjacency matrix: $C_{i,j} = 1$ if and only if $A_{i,j} > 0$. We use the function $ceil(\cdot)$ to denote the element-wise round-up to the nearest integer function. Then we normalize,

$$D_{i,j} = \frac{C_{i,j}}{\sum_j C_{i,j}}, \quad \text{and} \quad \overline{D}_{i,j} = \frac{C_{j,i}}{\sum_i C_{i,j}}, \tag{25}$$

and construct the matrix

$$\overline{R} = \frac{(D + \overline{D})}{2}. \tag{26}$$

This mimics the methods of the reversed Markov chain (19) and (20), but is built of stochastic matrices D and $\overline{D}$. In this case, transition weights emphasize actual transitions with respect the topological dynamics of the dynamical system, rather than by invariant probability associated with the dynamics. Further, the possible division by zero values of p_i in (19) is avoided.

We proceed to investigate the second eigenvector v_2 of $\overline{R}$. In Fig. 6, we illustrate a signs vector associated with v_2,

$$\sigma = \text{sign}(v_2 - q), \tag{27}$$

where q is a scalar $-1 \leq q \leq 1$ chosen so that the area flux of each signed region is balanced. The color scheme in Fig. 6 is chosen so that those cells B_i such that $\sigma_i > 0$ are colored blue, and otherwise red, whence we denote the vector partition,

$$\sigma = \sigma_+ + \sigma_-. \tag{28}$$

In this notation, balance may be formulated as $R\sigma_+ \simeq R\sigma_-$ which is a statement of almost invariance.

It is instructive to compare Fig. 3 with the regions partitioned in Fig. 6, which are the FTLE and transfer operator analyses developed around data sets using the same exact 3-day time epochs. Whereas FTLE analysis is considered appropriate for discussion of transport pseudo-barriers, we see similar structures from the spectral theory of the Fröbenius–Perron operator corresponding to almost invariant sets. It is not surprising that these similar structures correspond to the interiors of the bounding ridges of the FTLE field. It is apparent that global analysis of the time-varying vector field can lead to a better understanding of the fate of oceanographic gyres, which are themselves time varying. As such, advection of pollutants, temperature variations, and ecological factors such as plankton blooms can all be better understood in terms of the time evolution of the bounding barriers and regions of almost invariance. As the analysis in this paper suggests, these can be defined in terms of adjustments to recently advanced tools in the theory of computational measurable dynamical systems.

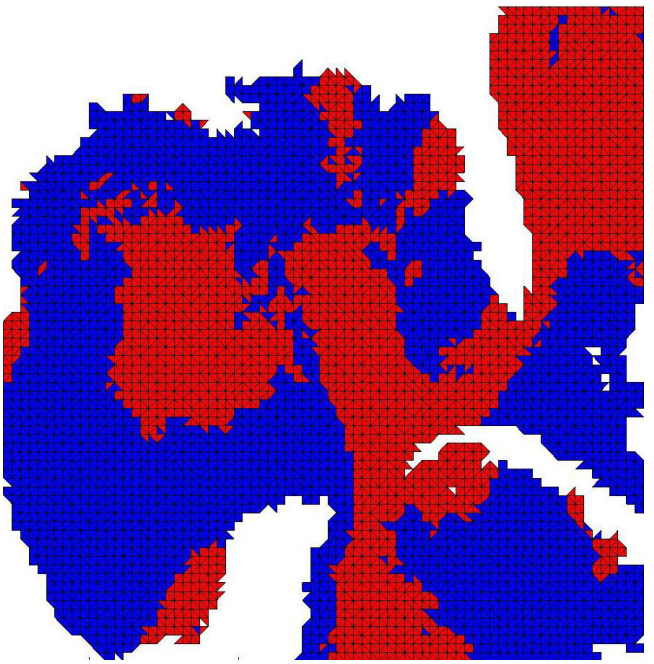

Fig. 6. Partition of the Gulf of Mexico using transfer operator approach. Regions in red correspond to almost-invariant sets, i.e. areas into and out of which little transport occurs.

5. Conclusions

Based on vector fields generated from a standard ocean model, we have used modern methods of computational and applied measurable dynamics to study the global dynamics related to the transport behavior in the Gulf of Mexico during the period of the Deep Water Horizon oil spill. Transfer operators and FTLE methods give complementary descriptions of the transport mechanisms, almost invariant sets, and the changing barriers associated with the

time dependence of this highly complex and nonautonomous dynamical system.

Initial predictions [NCAR, 2010], showed the oil quickly reaching the Gulf loop current and be carried as far north as Cape Hatteras, N.C. This loop current can be seen simply by inspecting the vector field in Fig. 2. This was not actually realized, as by mid-summer a circulation loop known as "Eddy Franklin" developed in the central Gulf, barring a large amount of oil from entering the Gulf Stream. The "Eddy Franklin" periodically sheds off the loop current and forces the northernmost point of the loop current much farther south. This particular eddy is known to form somewhat predictably, on average, once a year. However, there is no seasonal preference as to when it forms [Auer, 1987]. Because of the impossibility of forecasting ocean currents months into the future, the original NCAR model did not account for this phenomenon. Nonetheless, the phenomenon was factored into the modeled flow field later in the summer, and its consequences can be seen in the FTLE fields computed for the Gulf by early July (see [Bollt *et al.*, 2010]).

Our global analysis of this data set corroborates this behavior, as it is apparent that barriers to broader oil spread are formed early and strengthened throughout the summer. The formation of this eddy was shown in Fig. 5, can be seen in the resulting movie (which can be found online at [Bollt *et al.*, 2010]), and is apparent in the FTLE barriers. The timing of this eddy was rather fortunate for the east coast as it kept a barrier for transport out of the gulf in place, as seen in the FTLE. In summary, the global analysis of this paper offers a more proactive analysis for predicting the important understanding of future oceanographic agents' spreading.

Acknowledgments

This work was supported by the Office of Naval Research under grant #N00014-09-1-0647. The authors would also like to thank the anonymous referee for helpful comments and suggestions on the manuscript.

References

Aigner, E., Burgess, J., Carter, S., Nurse, J., Park, H., Schoenfeld, A. & Tse, A. [2010] "Tracking the oil spill in the gulf," http://www.nytimes.com/interactive/2010/05/01/us/20100501-oil-spill-tracker.html.

Auer, S. [1987] "Five-year climatological survey of the Gulf Stream system and its associated rings," *J. Geophys. Res.* **92**, 709–711,726.

Bleck, R. [2002] "An oceanic circulation model framed in hybrid isopycnic Cartesian coordinates," *Ocean Model.* **4**, 55–88.

Bollt, E., Billings, L. & Schwartz, I. [2002] "A manifold independent approach to understanding transport in stochastic dynamical systems," *Physica D* **173**, 153–177.

Bollt, E., Luttman, A., Kramer, S. & Basnayake, R. [2010] "FTLE field for Gulf of Mexico, summer 2010," http://people.clarkson.edu/∼aluttman/Gulf-FTLE.mov.

Bollt, E. M. & Santitissadeekorn, N. [2012] *Applied Measurable Dynamics and Empirical Transport Study*: *Tools for Numerical Analysis of Mixing and Turbulence* (in progress).

Brémaud, P. [1999] *Markov Chains*: *Gibbs Fields*, *Monte Carlo Simulation*, *and Queues* (Springer-Verlag).

Chan, T. F., Gilbert, J. R. & Teng, S.-H. [1995] "Geometric spectral partitioning," Tech. rep., UCLA.

Chui, C., Du, Q. & Li, T. [1992] "Error estimates of the Markov finite approximation of the Frobenius Perron operator," *Nonlin. Anal.* **19**, 291–308.

Chung, F. R. K. [1997] *Spectral Graph Theory*, Regional Conference Series in Mathematics, Number 92 (American Mathematical Society).

Ding, J. & Zhou, A. [1994] "The projection method for computing multidimensional absolutely continuous invariant measures," *J. Statist. Phys.* **77**, 899–908.

Froyland, G. [2005] "Statistically optimal almost-invariant sets," *Physica D* **200**, 205–219.

Froyland, G. & Padberg, K. [2009] "Almost-invariant sets and invariant manifolds — Connecting probabilistic and geometric descriptions of coherent structures in flows," *Physica D* **238**, 1507–1523.

Golub, G. & Van Loan, C. F. [1996] *Matrix Computations*, 3rd edition, Johns Hopkins Studies in Mathematical Sciences (The Johns Hopkins University Press).

Haller, G. & Poje, A. C. [1998] "Finite time transport in aperiodic flows," *Physica D* **119**, 352–380.

Haller, G. [2000] "Finding finite-time invariant manifolds in two-dimensional velocity fields," *Chaos* **10**, 99.

Haller, G. [2002] "Lagrangian coherent structures from approximate velocity data," *Phys. Fluids* **14**, 1851.

Halliwell, G. R. [2004] "Evaluation of vertical coordinate and vertical mixing algorithms in the HYbrid-Coordinate Ocean Model (HYCOM)," *Ocean Model.* **7**, 285–322.

Hunt, F. [1996] "Approximating the invariant measures of randomly perturbed dissipative maps," *J. Math. Anal. Appl.* **198**, 534–551.

HYCOM [2010] "Hybrid Coordinate Ocean Model (HYCOM)," http://www.hycom.org/.

Lasota, A. & Mackey, M. [1994] *Chaos*, *Fractals*, *and Noise*: *Stochastic Aspects of Dynamics* (Springer).

Li, T. [1976] "Finite approximation for the Fröbenius-Perron operator: A solution to Ulam's conjecture," *J. Approx. Th.* **17**, 177–186.

Meiss, J. [1992] "Symplectic maps, variational principles, and transport," *Rev. Mod. Phys.* **64**, 795–848.

NCAR [2010] "National center for atmospheric research website dedicated to spill deepwater horizon oil spill," http://www2.ucar.edu/news/ocean-currents-likely-to-carry-oil-spill-along-atlantic-coast.

Newman, M. [2004] "Fast algorithm for detecting community structure in networks," *Phys. Rev. E* **69**.

Newman, M. E. J. [2006] "Finding community structure in networks using the eigenvectors of matrices," *Phys. Rev. E* **74**.

Preis, R. & Dellnitz, M. [2003] *Congestion and Almost Invariant Sets in Dynamical Systems*, Proceedings of Symbolic and Numerical Scientific Computation (SNSC'01) (Springer).

Shadden, S., Lekien, F. & Marsden, J. [2005] "Definition and properties of Lagrangian coherent structures from finite-time Lyapunov exponents in two-dimensional aperiodic flows," *Physica D* **212**, 271–304.

Shadden, S., Dabiri, J. & Marsden, J. [2006] "Lagrangian analysis of fluid transport in empirical vortex ring flows," *Phys. Fluids* **18**, 047105.

Shadden, S. C., Lekien, F., Paduan, J. D., Chavez, F. P. & Marsden, J. E. [2009] "The correlation between surface drifters and coherent structures based on high-frequency radar data in Monterey Bay," *Deep Sea Res. Part II*: *Top. Stud. Oceanogr.* **56**, 161–172.

Ulam, S. M. [1970] *Problems in Modern Mathematics*, Science Editions (Wiley, NY).

Wheeden, R. L. & Zygmund, A. [1977] *Measure and Integral*: *An Introduction to Real Analysis*, Pure and Applied Mathematics (Marcel Dekker, Inc.).

Wiggins, S. [1992] *Chaotic Transport in Dynamical Systems* (Springer).